



International Journal of Communication Networks and Information Security

ISSN: 2073-607X, 2076-0930

Volume 15 Issue 01 Year 2023

Prediction of Alzheimer's Disease Using LeNet-CNN Model with Optimal Adaptive Bilateral Filtering

Dr. M.V.Vijaya Saradhi

Department of CSE, ACE Engineering College, Ghatkesar, Hyderabad, Telangana, India
meduri.vsd@gmail.com

Dr. Pinagadi Venkateswara Rao

School of Engineering, Mall Reddy University, Dulapally, Hyderabad, Telangana, India
drp.venkateswara@mallareddyuniversity.ac.in

Dr. V. Gokula Krishnan

Department of CSE, Saveetha School of Engineering, Saveetha Institute of Medical and Technical Sciences, Thandalam, Chennai, Tamil Nadu, India
gokul_kris143@yahoo.com

K.Sathyamoorthy

Department of CSE, Panimalar Engineering College, Poonamallee, Chennai, Tamil Nadu, India

pitsathyamoorthy@gmail.com

Dr. V. Vijayaraja

Department of AIDS, R M K College of Engineering and Technology, Kavaraipettai, Tamil Nadu, India

vijayarajaads@rmkcet.ac.in

Article History	Abstract
Received: 01 March 2023 Revised: 18 April 2023 Accepted: 16 May 2023	Alzheimer's disease is a degenerative dementia that causes progressively worsening memory loss and other cognitive and physical impairments over time. Mini-Mental State Examinations and other screening tools are helpful for early detection, but diagnostic MRI brain analysis is required. When Alzheimer's disease (AD) is detected in its earliest stages, patients may begin protective treatments before permanent brain damage has occurred. The characteristics of the lesion sites in AD affected role, as identified by MRI, exhibit great variety and are dispersed across the image space, as demonstrated in cross-sectional imaging investigations of the disease. Optimised Adaptive Bilateral filtering using a deep learning model was suggested as part of this study's approach toward this end. Denoising the pictures with the help of the suggested adaptive bilateral filter (ABF) is the first stage. The ABF improves denoising in edge, detail, and homogenous areas separately. After then, the ABF is given a weight, and the Adaptive Equilibrium Optimizer (AEO) is used to determine the best possible value for that weight. LeNet, a CNN model, is then used to complete the AD organisation. The first step in using the LeNet-5 network model to identify AD is to study the model's structure and parameters. The ADNI experimental dataset was used to verify and compare the suggested technique to other models. The experimental findings prove that the suggested method can achieve a classification accuracy of 97.43%, 98.09% specificity, 97.12% sensitivity, and 89.67% Kappa index. When compared against competing algorithms, the suggested model emerges victorious.

CC License
CC-BY-NC-SA 4.0

Keywords: Alzheimer's Disease, Adaptive Bilateral Filter, Adaptive Equilibrium Optimiser, LeNet, Convolutional Neural Network

1. Introduction

Healthcare in the twenty-first century faces significant challenges, chief among them Alzheimer's disease (AD), the most prevalent type of dementia. AD is the sixth most significant cause of States, affecting an estimated 5.5 million individuals aged 65 and over. The total annual cost of caring for people with AD in the United States in 2018 was \$277 billion [1], [2], putting a significant strain on the country's economy and the nation's healthcare system due to the high expense of medical treatment and other assistance programmes for patients and their families. There is currently no recognised disease-modifying therapy for AD, an irreversible, degenerative brain condition characterised by deterioration in cognitive ability [3]. For this reason, a lot of research has gone into pre-symptomatic early detection technologies to slow or prevent the course of illness. In particular, state-of-the-art neuroimaging methods have been developed and exploited to detect anatomical and molecular biomarkers associated with Alzheimer's disease (AD) [4], [5]. Data integration of methods [6], [7] resulted in an explosion of enthusiasm for using machine learning on computers to do integrative analysis. Popular pattern analysis techniques have shown promise in early AD detection and prediction of AD progression [8-10].

Using these machine learning techniques requires a well-defined architecture or set of pre-processing processes [11]. Four steps—features are often included in machine learning classification research. These methods may be time-consuming, requiring specialised expertise and several optimisation iterations. It has been highlighted that these procedures are difficult to replicate [12].

Deep learning approaches strategies for overcoming these obstacles. There has been an uptick in research using convolutional neural networks (CNN) in tandem with MRI imaging to detect AD in its earliest stages [14]. The typical CNN network has three layers: input, hidden, and output. When data is sent to the network, it is received by the input layer. Multiple convolutional and pooling layers make up the hidden layer. It is designed to do one thing: take input photographs and pull out their layered elements. Extracting the image's higher-level characteristics is a multi-step process that this hierarchical structure facilitates. The following are some drawbacks of these approaches: Because of the many layers that make up a conventional CNN, too deep networks may have the opposite effect of what was intended [15], [16]. Furthermore, conventional CNN does not preserve picture quality when subjected to an affine transformation. The flawed CNN functionality results from its default sampling strategy (matrix sampling).

To cleanse AD pictures of noise, this study employs a pre-processing technique based on optimal adaptive bilateral filtering. Applying AEO reduces the filtering burden. The LeNet structure is used to categorise AD to solve the conventional CNN's drawback. In Section 2, provide a list of works that are relevant to the proposed paradigm. Sections 3 and 4 detail the proposed model's explanation and validation. Finally, Section 5 concludes the research work.

2. Related Works

The most well-known DL models and the outcomes of implementing them are described by Hazarika et al. [17] in the context of AD organisation. All MR images of the brain are collected from the database. The DenseNet-121 model produces the most effective outcome, with an average performance rate of 88.78% compared to the other models presented. Although it outperforms many other models, the DenseNet's heavy reliance on convolutional processes makes it computationally sluggish. One common technique for improving the efficiency of a convolutional operation is called "depth-wise convolution." To reduce the running time, use depth-wise convolution layers instead of the original ones. The new design generally increased the efficiency of the perfect by 90.22 percent.

Helaly et al. [18] have developed a comprehensive framework for the diagnosis of Alzheimer's disease at any stage and the categorisation of medical images according to those diagnoses. In this study, use (CNN). The spectrum of AD may be broken down into four distinct phases. Each pair of AD stages is also classified using a binary system distinct from the other pairs. AD is detected by using two different approaches for classifying medical pictures. The COVID-19 pandemic has made it more difficult than ever to avoid the hospital due to crowding and disease. Due to this, we propose a web-based programme that employs the final qualifying suggested architectures for Alzheimer's

disease testing. Physicians and patients may benefit from remote monitoring of AD symptoms. In addition, it utilises the AD spectrum to identify the patient's position on the spectrum and provide advice according to that position. Each method is evaluated and compared using nine distinct metrics of performance.

Using deep learning can be used to create precise illness classification models is the goal of a unique three-step technique (SWAT-CNN) proposed by Jo et al. [19]. First, a convolutional neural network (CNN) was used on each non-overlapping piece of the complete genome to identify phenotype-associated regions. A Sliding Window Association Test (SWAT) was then used to run CNN on the chosen pieces to determine phenotypic influence scores (PIS) and locate SNPs related to the trait. Next, the model built a classification model by running CNN on all the SNPs it found. $N = 981$; cognitively normal older people from the Alzheimer's Disease Neuroimaging Initiative (ADNI) were used to evaluate our method. Our method can narrow the most critical genetic locus for AD to the already-famous APOE area. An area under the curve (AUC) of 0.82 was reached by our classification model, which was consistent with classical machine learning techniques such as random forest and XGBoost. AD-associated AD was discovered using SWAT-CNN, a deep revolutionary technique that shows promise for various medicinal applications.

A unified Fisher score and selection strategy has been developed by Sheng et al. [20]. To address the issue of the drastic gap between the feature scales of genetic and brain imaging, first learnt genetic features using the Fisher score and then dimensionality reduction to bridge the gap. Next, learn the characteristics associated between brain imaging and genetic data and use those weight coefficients to multiply the traits. Five imaging characteristics and five genetic features were chosen by the feature selection software to produce. The classification accuracy was enhanced somewhat compared to when just imaging data were used; moreover, a collection of connected features of brain imaging phenotypes and genetic variables was chosen to enhance the classification accuracy further.

In the research by Savaş [21], brain MRIs were used to categorise the antecedent phases of Alzheimer's disease as usual, moderate cognitive impairment, and Alzheimer's disease. Classification of 2182 picture objects from the ADNI database was accomplished using several models based on the CNN architecture. The results of the comparison of 29 pre-trained models' image-processing abilities were reported in this research. Each model's accuracy value was calculated, as were the precision, specificity, and sensitivity rates for each class. When put to the test, the EfficientNetB0 model performed with a 92.98% success rate, making it the most accurate. EfficientNetB3 (97.28%) models obtained the most excellent rates of accuracy (89.78%), sensitivity (94.42%), and specificity (97.28%) of the Alzheimer's disease class during the comparative assessment stage using the confusion matrix. The research found that compared to other pre-trained models, EfficientNet models performed the best in classification accuracy.

Hippocampal atrophy is the most reliable clinical sign of Alzheimer's disease, and Liang et al. [22] have proposed a new technique for identifying AD patients based on this symptom. A total of 207 patients with (AD), 209 patients with moderate cognitive impairment (MCI), and 109 cognitively normal (CN) individuals were analysed using T1-weighted MRIs from the ADNI dataset. First, MRI images are segmented to isolate the left and right hippocampus; then, feature extraction using PCANet is performed; lastly, the Broad Learning System (BLS) categorises patients into distinct groups. The PCANet approach can efficiently extract the most relevant features from images. At the same time, the BLS method can achieve over 95% accuracy and in a shorter amount of time than traditional machine learning techniques. Experimental results have revealed that our method improves the precision and throughput of the classification task in AI-assisted Alzheimer's disease diagnosis. In [26], a modified EfficientNet for three-dimensional space predicts AD. The multiscale characteristics of brain MRI are explored by mobile inverted bottleneck convolution with modified EfficientNet. The model is tested with four classification stages of AD.

3. Proposed System

3.1 Data Selection

ADNI data was utilised for this analysis (<http://adni.loni.usc.edu>, accessed on 16 February 2020). Normal controls (NC), moderate cognitive impairment (MCI), and (AD) are the three broad classifications used to analyse the dataset (AD). The onset of MCI marks a significant point from average to AD functioning. The study tested 515 samples, 55 of which were diagnosed with

Alzheimer's disease (AD), 255 with normal cognitive function (NC), and 205 with mild cognitive impairment (MCI). Nearly as many men as women belonged to each group. To get a score on the MMSE scale, clinicians need to ask patients a series of questions. The score on the scale may be any positive or negative integer between 0 and 30. A higher score indicates better health, whereas a lower number indicates more severe dementia. Scoring between 24 and 30 on the MMSE and less than 12 on the ADAS-Cog indicates NC. The MMSE range for MCI is 23-30, whereas the ADAS-Cog range is 7-17. Those with an MMSE score between 20 and 26 and an ADAS-Cog score between 12 and 29 have AD [24]. Table 1 displays the information that was gathered.

Table 1. Info of ADNI Dataset Used in this Study

Diagnosis	MCI	NC	AD
Age	73.8 ± 7.5	70.6 ± 5.1	78.9 ± 8.6
ADAS-Cog	7-17	<12	12-29
Number of male samples	102	128	28
Sum of samples	205	255	55
The sum of female samples	103	127	27
MMSE	23-30	24-30	20-26

3.2 Pre-processing

3.2.1 Data Normalisation

There is also a normalisation of picture values, and two methods of improving image quality have been investigated. 3D volume pictures are normalised to the [0,1] range in their basic form. When in a different arrangement, it strains against contrast. To normalise the volume to the [0, 1] range, the 2nd and 98th percentile values are determined and assigned as the minimum and maximum, respectively.

3.2.2 Denoising Filters Using Traditional Bilateral Filtering (TBF)

Detail loss is a significant issue with denoising filters. And the techniques can't tell the difference between an edge and a consistent pixel. For this reason, a technique that can modify the level of smoothing depending on picture areas is required. This work proposes a novel CV-based approach to noise picture classification, dividing it into homogeneous, detailed, and edge areas. As a result, the bilateral filter may be used in various contexts and settings. The following model is most applicable for photos containing multiplicative noise, as shown in Equation (1).

$$f(x, y) = g(x, y) \cdot \eta_m(x, y) + \eta_a(x, y) \quad (1)$$

Where $f(x,y), g(x,y), \eta_m(x,y)$ and $\eta_a(x,y)$ multiplicative and additive noise functions, and the actual noisy picture and unknown noise-free image. In order to account for the speckle noise in an ultrasonic picture, the study uses Equation (2), which takes into account the fact that additive noise is often thought to be less than noise.

$$f(x, y) = g(x, y) \cdot \eta_m(x, y) \quad (2)$$

Ultrasound pictures include speckle noise, which is multiplicative noise. So, a logarithmic transformation of the noisy picture is recommended. So, as the following Equation (3) demonstrates, multiplicative noise has a high potential for addiction.

$$\log f(x, y) = \log(g(x, y)) \cdot \log(\eta_m(x, y)) \quad (3)$$

Coefficient of Variation

The CV is unit less. Therefore, the value is the same for significant and slight variations in high and low-intensity areas. This results in the same function being used for areas of varying brightness. In this sense, CV outperforms the standard deviation. The CV formula is mentioned in Equation (4):

$$CV = \frac{S_a}{m_a} \times 100 \quad (4)$$

Where S_a and m_a Mean and standard deviation are and, respectively. Therefore, "Edges", "Homogenous", and "Detail" correlate to high, low, and intermediate CV values.

3.2.3 Adaptive Bilateral Filter

Using the suggested ABF, the study modified the TBF such that its characteristics vary depending on the area being analysed. Adjustments to the bilateral filter's window size, intensity dispersion, and spatial dispersion are as follows in Equations (5-7).

$$\sigma(d)_{ij} = \sigma_d \times (1 - CV_{ij}) \quad (5)$$

$$\sigma(r)_{ij} = \sigma_r \times (1 - CV_{ij}) \quad (6)$$

$$w_{ij} = \left(2 \times \left(\sigma_d \times (1 - CV_{ij}) \right) \right) + 1 \quad (7)$$

Where $(d)_{ij}$ and $(r)_{ij}$ are the variances in space and intensity for the applied i, j pixels. The W^*W size is denoted by w_{ij} . The performance of the bilateral filter may be enhanced by localising the variances and the window size. The bilateral filter is most sensitive to changes when the CV_{ij} value is close to one. As a result, w_{ij} , r_{ij} , and d_{ij} are all reduced by the suggested ABF. Reduced values of $(d)(r)(w)_{ij}$ are effective in restoring sharp borders. Further, the bilateral filter is close to the homogeneous regions when CV_{ij} is close to zero. As a result, ABF boosts (d) , (r) , and $(w)_{ij}$. Homogeneous regions become less distinct as $(d)_{ij}$, $(r)_{ij}$, and w_{ij} get larger.

Weighted Adaptive Bilateral Filter

The study will assign big weights to surround coefficients quite different in size from one another and small weights to those very close in magnitude. While detail pixels cluster together and remain stable, noisy ones are scattered or intermittent. Because values at neighbouring places tend to be more consistent, the study uses a measure of value similarity called $W(x,y)$, where x and y are coordinates. It is shown in Equations (8-9):

$$G_{\sigma(d)_{ij}} = G_{\sigma(d)_{ij}}(\|p - Q\|) \times W(x,y) \quad (8)$$

$$W(x,y) = \text{EXP} \left(- \left(\frac{I(x,y) - I(x+r,y+s)}{C_{\sigma}} \right)^2 \right) \quad (9)$$

Where $G_{\sigma(d)_{ij}}(\|p - Q\|)$ is the spatial weight of bilateral filter, $I(x,y)$ and $I(x+r,y+s)$ are central coefficients and neighbor coefficients. The window size of the denoising filter $W(x,y)$ is w , where $w = w$. Since less-noisy regions tend to be more distinct. As a result, it modifies the effectiveness of this filter by dampening it in quiet environments and amplifying it in noisier ones. The Eq. (10-12) specified it.

$$N = 10 \times \text{noise-est} \times K \quad (10)$$

$$M = \left(\text{Sigmf} \left(N, \left[1, \frac{K}{2} \right] \right) \right)^4 \quad (11)$$

$$\begin{cases} W_{xy} = W_{xy} - (1 - M) \times (W_{xy} - 1), & W_{xy} > 1, \\ W_{xy} = W_{xy} + (1 - M) \times (1 - W_{xy}), & W_{xy} \leq 1 \end{cases} \quad (12)$$

Where "noise-est" is the image noise variance estimate, N is the image noise normalisation in the interval $[0, K]$, and Sigmf is the sigmoid function. Filter effects at their maximum intensity for noise-est:1 result in the value 10. It is discussed how AEO chooses the best window size for the adaptive filter.

3.2.3.1 Adaptive Equilibrium Optimiser

It is suggested that this algorithm carries out the best solution for the window size of bilateral filtering. One step beyond the equilibrium optimiser is the adaptive equilibrium optimiser [25]. The search agents in this method are randomly dispersed in a search space determined by the fitness metric. The equilibrium and the dynamic condition that relies on the mass preservation law by exiting, creating, and entering the control volume encourage the equilibrium optimiser.

First, the search agents are connected to the density of the search space, with the iteration starting at $it = 1$.

$$Z_j(\text{itr} = 1) = l_b + \text{rand}_j(1, e) * (u_b - l_b), j = 1, 2, \dots, M \quad (13)$$

Lower and upper limits for the search space are denoted by l_b and u_b in Eq. (13), M denotes search agents, the problem dimension is denoted by e , and the random integer between 0 and 1 is denoted by rand_j in the 1-D vector. In the equilibrium optimiser, the position of the j th search agent is modified according to the value of the control volume C_v as in Equation (14):

$$\vec{Z}_j(\text{new}) = \vec{Z}_{\text{eq}}(\text{itr}) + \left(\vec{Z}_j(\text{itr}) - \vec{Z}_{\text{eq}}(\text{itr}) \right) * \vec{E}_j(\text{itr}) + \frac{g_j(\text{itr})}{\eta_j(\text{itr}) * C_v} \times (1 - \vec{E}_j(\text{itr})) \quad (14)$$

$Z_{\text{eq}}^{\rightarrow}$ determines the equilibrium! Z_{eq} pool of the four best search agents $Z_{\text{eq}}^{\rightarrow}(\text{eq}(1))$, $Z_{\text{eq}}^{\rightarrow}(\text{eq}(2))$, $Z_{\text{eq}}^{\rightarrow}(\text{eq}(3))$, and $Z_{\text{eq}}^{\rightarrow}(\text{eq}(4))$, and the average is described as $Z_{\text{eq}}^{\rightarrow}(\text{avg})$. The values of! $Z_{\text{eq}}^{\rightarrow}(\text{eq}(1))$, $Z_{\text{eq}}^{\rightarrow}(\text{eq}(2))$, $Z_{\text{eq}}^{\rightarrow}(\text{eq}(3))$, and $Z_{\text{eq}}^{\rightarrow}(\text{eq}(4))$ are chosen by the fitness values such as $Z_{\text{eq}}^{\rightarrow}(\text{eq}(1))$, $Z_{\text{eq}}^{\rightarrow}(\text{eq}(2))$, $Z_{\text{eq}}^{\rightarrow}(\text{eq}(3))$, and $Z_{\text{eq}}^{\rightarrow}(\text{eq}(4))$. The ranked list is used to ascertain fitness values and equilibrium candidates for the minimisation problem. Each of the M search agents' fitness values is characterised by Equations (15-16):

$$F = (F_1, F_2, \dots, F_3) \quad (15)$$

$$[\text{sorted}_F, \text{sort}_{\text{index}}] = \text{sort}(F) \quad (16)$$

These fitness values, together with the equilibrium candidates, are now represented by Equation (17):

$$\begin{aligned} F(\vec{Z}_{\text{eq}(1)}) &= \text{sorted}_{F(1)} \text{ and } \vec{Z}_{\text{eq}(1)} = \vec{Z}(\text{sorted}_{F(1)}) \\ F(\vec{Z}_{\text{eq}(2)}) &= \text{sorted}_{F(2)} \text{ and } \vec{Z}_{\text{eq}(2)} = \vec{Z}(\text{sorted}_{F(2)}) \\ F(\vec{Z}_{\text{eq}(3)}) &= \text{sorted}_{F(3)} \text{ and } \vec{Z}_{\text{eq}(3)} = \vec{Z}(\text{sorted}_{F(3)}) \\ F(\vec{Z}_{\text{eq}(4)}) &= \text{sorted}_{F(4)} \text{ and } \vec{Z}_{\text{eq}(4)} = \vec{Z}(\text{sorted}_{F(4)}) \\ \vec{Z}_{\text{eq}(\text{avg})} &= \frac{1}{4} (\vec{Z}_{\text{eq}(1)} + \vec{Z}_{\text{eq}(2)} + \vec{Z}_{\text{eq}(3)} + \vec{Z}_{\text{eq}(4)}) \end{aligned} \quad (17)$$

Ultimately, as:

$$\vec{Z}_{\text{eq},\text{pool}} = \{ \vec{Z}_{\text{eq}(1)}, \vec{Z}_{\text{eq}(2)}, \vec{Z}_{\text{eq}(3)}, \vec{Z}_{\text{eq}(4)}, \vec{Z}_{\text{eq}(\text{avg})} \} \quad (18)$$

The exponential factor $E_{\rightarrow j}$ is to help the equilibrium optimiser exploration is computed for the j th search agents as

$$\vec{E}_j(\text{itr}) = x_1 \text{ sign}(s_1 - 0.5) \left[e^{-\eta_j \left(1 - \frac{\text{itr}}{\max_itr} \right)^{\left(x_2 \frac{\text{itr}}{\max_itr} \right)}} \right] \quad (19)$$

Based on Eq. (19), the exploration function is controlled by the factor x_1 , the exploitation function is controlled by the factor x_2 , the factor sign controls the search direction, and the arbitrary vector of dimension in the range 0 to 1 for the j th search agent in its iterations is represented by the symbol $_j(\text{itr})$. The current iteration number is represented by the symbol itr and the maximum iteration sum.

The generation rate $g_{\rightarrow j}(\text{itr}) = g_{\rightarrow j,0}(\text{itr}) * E_{\rightarrow j}(\text{itr})$ assists the exploration stage using participation probability $Z_{\text{eq}}^{\rightarrow}$.

The $g_{\rightarrow j}$ is described as in Equation (20):

$$\vec{g}_j(\text{itr}) = \vec{g}_{j,0}(\text{itr}) * \vec{E}_j(\text{itr}) \quad (20)$$

The $g_{\rightarrow j,0}(\text{itr})$ and $(\text{grc})_{\rightarrow j}(\text{itr})$ are computed as in Equations (21-22):

$$\vec{g}_{j,0}(\text{itr}) = \overline{\text{grc}}_j(\text{itr}) (\vec{Z}_{\text{eq}}(\text{itr}) - \vec{\eta}_j(\text{itr})) \quad (21)$$

$$\overline{\text{grc}}_j(\text{itr}) = \begin{cases} 0.5 & s_1 \geq g_p \\ 0 & s_2 \geq g_p \end{cases} \quad (22)$$

grc stands for the generation rate control factor, g_p for the probability, s_1 and s_2 for random values between 0 and 1, and so on. All search agents' current and average fitness is used to make the adaptive choice, and the minimisation problem is stated in Equation (23).

$$\vec{Z}_j(\text{itr} + 1) = \begin{cases} \vec{Z}_j(\text{new}) & F_j(\text{itr}) < F_{\text{avg}}(\text{itr}) \\ \vec{Z}_j(\text{new}) \otimes (0.5 + \text{rand}(1, e)) & F_j(\text{itr}) < F_{\text{avg}}(\text{itr}) \end{cases} \quad (23)$$

Fitness values for each search agent are denoted by $F_j(\text{itr})$ and $F_{\text{avg}}(\text{itr})$, respectively; Eq. (23) denotes component-wise multiplication.

$$F_{avg}(itr) = \frac{1}{M} \sum_{j=1}^M F_j(itr) \quad (24)$$

The notions of memory storage are transferred from the equilibrium optimiser to the adaptive equilibrium optimiser. Therefore, after the optimum fitness value has been found, the current iteration is compared to the previous one and the formula changes. Equations (25-26) state that:

$$\bar{Z}_j(itr) = \begin{cases} \bar{Z}_j(itr) & itr > 1 \text{ and } F_j(itr) < F_j(itr - 1) \\ \bar{Z}_j(itr - 1) & itr > 1 \text{ and } F_j(itr) \geq F_j(itr - 1) \\ \bar{Z}_j(itr) & itr = 1 \end{cases} \quad (25)$$

And $F_j(itr)$

$$F_j(itr) = \begin{cases} F_j(itr) & itr > 1 \text{ and } F_j(itr) < F_j(itr - 1) \\ F_j(itr - 1) & itr > 1 \text{ and } F_j(itr) \geq F_j(itr - 1) \\ F_j(itr) & itr = 1 \end{cases} \quad (26)$$

By identifying the optimal solution using the algorithm, the control parameters are selected effectively, which leads to filtering the noises for final classification.

3.3 Classification for AD

Many deep learning methods have been developed for use in real-time systems. Among these methods, Convolutional Neural Network (CNN) has quickly become the go-to for everything from vision system design and implementation to medical image construction. Alzheimer's disease (AD) in medical imaging was initially classified using the LeNet-5 CNN architecture.

A. First Layer:

A 32x32 grayscale AD picture was fed into the LeNet-5 CNN model through the first convolutional layer, with a filter size of 5x5 and a stride value of 1.

B. Second Layer:

A median pooling layer was added to the LeNet-5 CNN model, and a 22 filter with a 2 strides value was used.

C. Third Layer:

A convolutional layer with 16 filters of 5x5 dimensions and a stride of one was added into the third layer of the LeNet-5 architecture.

D. Fourth Layer:

Again, a layer of average pooling with a 22 kernel and a stride value of 2 made up the fourth layer.

E. Fifth Layer:

Each kernel in the fifth, fully linked layer of the LeNet-5 architecture was 55 units in size. There was a direct connection between each node in the fourth layer and each of the 120 units in this layer.

F. Sixth Layer:

With 84 units, the LeNet-5 model's sixth layer was wholly linked.

G. Output Layer

Finally, a fully-connected sigmoid output layer was used to classify people as either AD or non-AD.

The study found that applying the activation function ReLu helped us the most. The study trained the model 157 times with a batch size of 32. A summary of LeNet's architecture is provided in Table 2.

Table 2. Summary of Model

Layer	Activation	Sum of Filter	Stride	Filter Size	Output Shape
Image	-	1	-	-	32x32
Convolution	relu	6	1	5x5	32x32
Fully-Connected	relu	-	-	-	120
Fully-Connected	relu	-	-	-	84
Convolution	relu	16	1	5x5	12x12
Average Pooling	relu	16	2	2x2	6x6
Average Pooling	relu	6	2	2x2	16x16
Fully-Connected	Sigmoid	-	-	-	2

4. Results and Discussion

Quantitative and qualitative evaluations of performance are included here. With 8GB of RAM, a 1TB hard drive, and a 3.0GHz Intel i5 CPU, the suggested system is built using Python and Pytorch.

4.1 Performance Metrics

This research provides the mathematical expressions for the following metrics: SPE, SEN, and ACC, which are provided in Equations (27-29).

$$ACC = \frac{TP+TN}{TP+TN+FP+FN} \quad (27)$$

$$SEN = \frac{TP}{TP+FN} \quad (28)$$

$$SPE = \frac{TN}{TP+FP} \quad (29)$$

In this case, the experiment analysis is conducted in two ways, with and without pre-processing, as indicated in Tables 3 and 4. Since segmentation models are employed by currently available methods and pre-processing models have received little attention, generic pre-trained models are considered for experimental analysis. But the suggested approach aimed to de-noise the AD pictures using optimum weighted adaptive bilateral filtering.

Table 3. Analysis of the Proposed Model without Pre-processing

Methodologies	Accuracy	Sensitivity	Specificity	Kappa Index
VGGNet	85.43	67.15	75.16	76.38
AlexNet	89.03	85.40	83.50	77.92
MobileNet	93.60	81.60	87.04	80.75
Proposed	94.70	89.80	96.44	85.17

In the accuracy analysis, the proposed model achieved 94.70%, VGGNet has 85.43%, and AlexNet has 89.03%. The specificity of the proposed model is 96.44%, the existing models, such as AlexNet and MobileNet, achieved nearly 85% of specificity, and VGGNet has 75.16% of specificity. Compared with all techniques, VGGNet achieved less performance, i.e., 67.15% of sensitivity and 76.38% of the Kappa index. AlexNet and MobileNet achieved 83% sensitivity and nearly 79% Kappa index. But the proposed model achieved 89.90% sensitivity and 85.17% Kappa index.

Table 4. Analysis of the Proposed Model with Pre-processing

Methodologies	Sensitivity (%)	Accuracy (%)	Specificity (%)	Kappa index (%)
VGGNet	90.14	91.22	97.24	79
AlexNet	94.03	90.89	96.69	79.08
MobileNet	94.76	93.98	95.30	83.44
Proposed	97.12	97.43	98.09	89.67

Comparing Table 3, the proposed model achieved 97.12% of sensitivity, 98% of specificity, 97.43% of accuracy and 89.67% of kappa index. The reason for better performance is the introduction of weighted adaptive bilateral filtering, and AEO selects the optimal weight of bilateral filtering. The proposed model and the existing models also increased their performance by introducing pre-processing models. For example, the existing models such as VGGNet, AlexNet and MobileNet achieved nearly 92% to 94% of sensitivity, 92% of accuracy, 95% to 97% of specificity and 79% to 83% of the Kappa index. Figure 1 to 4 provides a graphical comparison of the proposed model.

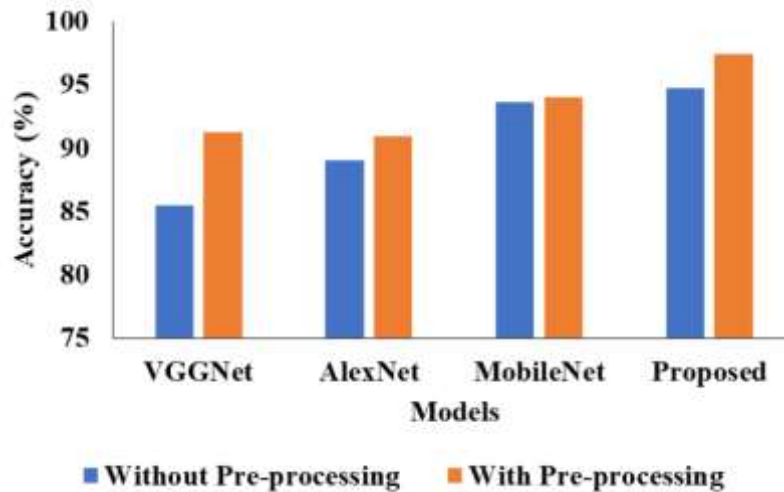


Figure 1. Accuracy Comparison

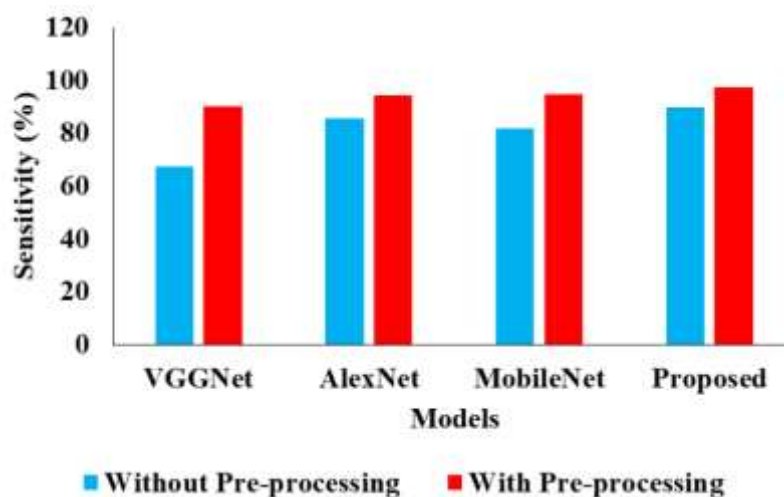


Figure 2. Sensitivity Comparison

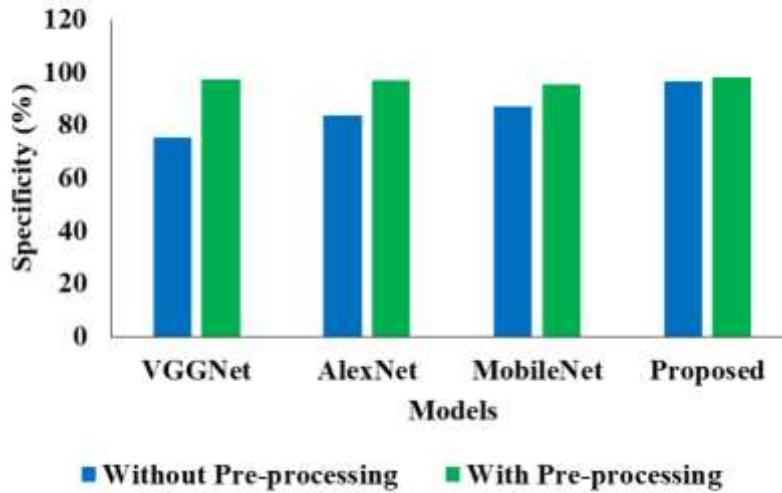


Figure 3. Specificity Comparison

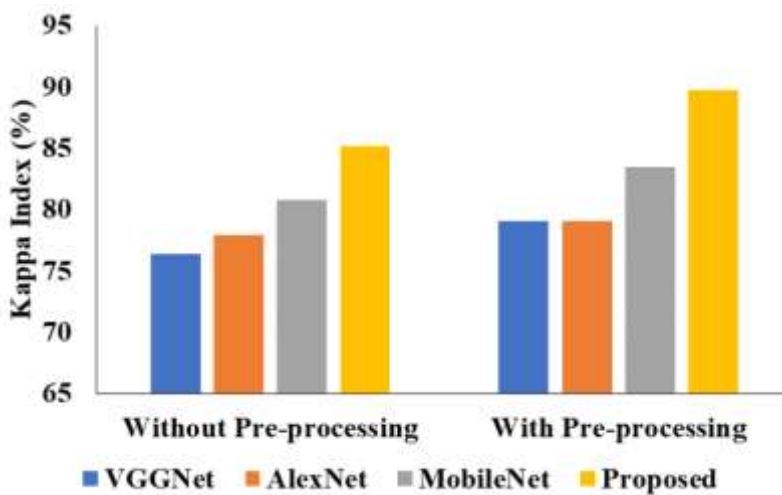


Figure 4. Kappa Index Comparison

5. Conclusion

The study suggests a deep learning perfect built on LeNet for early AD detection in this study. This paper introduces an AEO-based optimum adaptive bilateral filtering technique for noise reduction in AD images. With AEO, the adaptive bilateral filter's regulating parameter may converge more quickly. Adding Gaussian noise to the source picture at varying levels of noise variance results in a noisy AD image in the suggested technique. The optimal value of the adaptive bilateral filter's control parameters is then obtained by using an optimisation method. To ensure the efficacy of the suggested strategy, it was tested on the ADNI experimental dataset and associated with the existing models. The trial findings validate the superior performance and improved robustness of the proposed model in a clinical setting. That's proof of its effective pattern recognition. Model robustness may be improved with the addition of a pre-processing model. The classification accuracy of the method suggested in this research was found to attain 97.43% accuracy using the ADNI dataset, demonstrating the benefits of the proposed model. There is great potential for the suggested strategy in actual AD settings. Our subsequent studies will combine gene identification for AD susceptibility with pattern recognition.

References

- [1] Fong, J.X., Shapiai, M.I., Tiew, Y.Y., Batool, U. and Fauzi, H., "Bypassing MRI Pre-processing in Alzheimer's Disease Diagnosis using Deep Learning Detection Network," 2020 16th IEEE International Colloquium on Signal Processing & Its Applications (CSPA), *IEEE Access*, 2020, pp. 219-224.

- [2] De la Fuente Garcia, S., Ritchie, C.W. and Luz, S., "Artificial intelligence, speech, and language processing approach to monitoring Alzheimer's disease: a systematic review," *Journal of Alzheimer's Disease*, vol.78, no.4, 2020, pp.1547-1574.
- [3] Bäckström, K., Nazari, M., Gu, I. Y. H. and Jakola, A. S., "An efficient 3D deep convolutional network for Alzheimer's disease diagnosis using MR images," In 2018 IEEE 15th International Symposium on Biomedical Imaging (ISBI 2018), *IEEE*, 2018, pp.149-153.
- [4] Yagis, E., Citi, L., Diciotti, S., Marzi, C., Atnafu, S.W. and De Herrera, A. G. S., "3d convolutional neural networks for diagnosis of Alzheimer's disease via structural MRI." In 2020 IEEE 33rd International Symposium on Computer-Based Medical Systems (CBMS), *IEEE*, 2020, pp.65-70.
- [5] Marghalani, B.F. and Arif, M., "Automatic classification of brain tumour and Alzheimer's disease in MRI," *Procedia Computer Science*, vol.163, 2019, pp.78-84.
- [6] Liu, M., Cheng, D., Wang, K. and Wang, Y., "Multi-modality cascaded convolutional neural networks for Alzheimer's disease diagnosis." *Neuroinformatics*, vol.16, no.3, 2018, pp.295-308.
- [7] Khanna, A., Selvaraj, P., Gupta, D., Sheikh, T. H., Pareek, P. K., & Shankar, V., "The Internet of Things and deep learning enabled healthcare disease diagnosis using biomedical electrocardiogram signals," *Expert Systems*, 2021, p.e12864. Available: <https://doi.org/10.1111/exsy.12864>.
- [8] Roobini, M.S. and Lakshmi, M., "Diagnosis of Alzheimer's Disease using Classification Algorithms," In 2020 3rd International Conference on Intelligent Sustainable Systems (ICISS), *IEEE*, 2020, pp.725-734.
- [9] Venaktesh, C., Dr Ramana, L. Siva Yamini, Emad Abouel Nasr, Ali K. Kamrani, and Mohamed K. Aboudaif., "A neural network and optimisation based lung cancer detection system in CT images," *Frontiers in Public Health*, pp.188, 2022. Available: <https://doi.org/10.3389/fpubh.2022.769692>.
- [10] Suresha, H. S. and Parthasarathy, S. S., "Diagnosis of Alzheimer's disease using fast, independent component analysis and otsu multi-level thresholding." *International Journal of Intelligent Engineering and Systems*, vol.11, no.5, 2018, pp.74-83.
- [11] S. Kasthuri, Dr A. Nisha Jebaseeli, "An Artificial Bee Colony and Pigeon Inspired Optimization Hybrid Feature Selection Algorithm for Twitter Sentiment Analysis," *Journal of Computational and Theoretical Nanoscience*, P. No. 5378-5385, 2020, vol.17, no.12.
- [12] Hussain, E., Hasan, M., Hassan, S.Z., Azmi, T.H., Rahman, M.A. and Parvez, M.Z., "Deep learning-based binary classification for Alzheimer's disease detection using brain MRI images," In 2020 15th IEEE Conference on Industrial Electronics and Applications (ICIEA), *IEEE*, 2020, pp. 1115-1120.
- [13] Moore, P.J., Lyons, T.J., Gallacher, J. and Alzheimer's Disease Neuroimaging Initiative, "Random forest prediction of Alzheimer's disease using a pairwise selection from time series data," *PloS one*, vol.14, no.2, 2019, p.e0211558.
- [14] Leong, L. K. and Abdullah, A. A., "Prediction of Alzheimer's disease (AD) using machine learning techniques with the Boruta algorithm as a feature selection method," *Journal of Physics: Conference Series*, vol.1372, no.1, 2019, p.012065.
- [15] Paraskevaidi, M., Morais, C.L., Freitas, D.L., Lima, K.M., Mann, D.M., Allsop, D., "Martin-Hirsch, P.L. and Martin, F.L., Blood-based near-infrared spectroscopy for the rapid, low-cost detection of Alzheimer's disease," *Analyst*, vol.143, no.24, 2018, pp.5959-5964.
- [16] Wang, X. and Wang, W., "Adaptive Weights Integrated Convolutional Neural Network for Alzheimer's Disease Diagnosis." *Journal of Medical Imaging and Health Informatics*, vol.10, no.12, 2020, pp.2893-2900.
- [17] Hazarika, R.A., Kandar, D. and Maji, A.K., "An experimental analysis of different deep learning-based models for Alzheimer's disease classification using brain magnetic resonance images," *Journal of King Saud University-Computer and Information Sciences*, vol.34, no.10, 2022, pp.8576-8598.
- [18] Helaly, H.A., Badawy, M. and Haikal, A.Y., "Deep learning approach for early detection of Alzheimer's disease," *Cognitive Computation*, vol.14, no.5, 2022, pp.1711-1727.

- [19]Jo, T., Nho, K., Bice, P., Saykin, A.J. and Alzheimer's Disease Neuroimaging Initiative, "Deep learning-based identification of genetic variants: application to Alzheimer's disease classification," *Briefings in Bioinformatics*, vol.23, no.2, 2022, pp.bbac022.
- [20]Sheng, J., Xin, Y., Zhang, Q., Wang, L., Yang, Z. and Yin, J., "Predictive classification of Alzheimer's disease using brain imaging and genetic data," *Scientific Reports*, vol.12, no.1, 2022, pp.1-9.
- [21]Savaş, S., "Detecting the stages of Alzheimer's disease with pre-trained deep learning architectures," *Arabian Journal for Science and Engineering*, vol.47, no.2, 2022, pp.2201-2218.
- [22]Liang, C., Lao, H., Wei, T. and Zhang, X., "Alzheimer's disease classification from hippocampal atrophy based on PCANet-BLS," *Multimedia Tools and Applications*, vol.81, no.8, 2022, p.11187-11203. Available online: <http://adni.loni.usc.edu>. [accessed on 16 February 2020].
- [23]Liu, M., Li, F., Yan, H., Wang, K., Ma, Y., Shen, L. and Xu, M., "A multi-model deep convolutional neural network for automatic hippocampus segmentation and classification in Alzheimer's disease," *NeuroImage*, vol.208, 2020, p.116459.
- [24]Wunnava, A., Naik, M.K., Panda, R., Jena, B. and Abraham, A., "A novel interdependence-based multi-level thresholding technique using adaptive equilibrium optimiser," *Engineering Applications of Artificial Intelligence*, vol.94, 2020, p.103836.
- [25]Shamrat, F.J.M., Akter, S., Azam, S., Karim, A., Ghosh, P., Tasnim, Z., Hasib, K.M., De Boer, F. and Ahmed, K., "AlzheimerNet: An Effective Deep Learning based Proposition for Alzheimer's Disease Stages Classification from Functional Brain Changes in Magnetic Resonance Images." *IEEE Access*, 2023.